Decomposition of Dimethyl Methylphosphonate (DMMP) on Supported Cerium and Iron Co-Impregnated Oxides at Room Temperature

Mark B. Mitchell,* Viktor N. Sheinker, Aron B. Tesfamichael, Enid N. Gatimu, and Maya Nunley

Department of Chemistry and the Center for Surface Chemistry, Clark Atlanta University, Atlanta, Georgia 30314

Received: August 7, 2002; In Final Form: November 6, 2002

The adsorption and decomposition reactions of dimethyl methylphosphonate (DMMP) on cerium and iron oxides supported on aluminum oxide have been examined at 25 °C. The capacities of these solids for the decomposition of DMMP have been measured, and the identities and amounts of the decomposition products determined. The coimpregnated oxide formulations are significantly more reactive than alumina alone, and the current formulations are 2.5× more reactive at room temperature than any other metal oxide studied previously. A series of screening experiments show that the most active formulation is one containing 5 wt % iron and 7.5 wt % cerium. At 25 °C, Al_2O_3 shows a decomposition capacity of 317 μmol/g, while the alumina-supported iron and cerium oxide combination shows a decomposition capacity of more than 510 μmol/g. Formulations containing similar amounts of iron oxide or cerium oxide individually are more active than the unmodified alumina but less active than the coimpregnated oxide. The results show that the three-dimensional CeO_2 phase that forms when cerium oxide is impregnated on alumina by itself is inactive for decomposition, and that the increased reactivity for these materials originates with a two-dimensional cerium oxide phase. The increased activity for the materials that include iron is suggested to be due to the iron either increasing the number of defect sites in the ceria crystallites that do form, or facilitating the formation of smaller crystallites.

Introduction

The interactions and reactions of dimethyl methylphosphonate (DMMP) on metal oxide surfaces are important because DMMP serves as a simulant for pesticides and for chemical warfare agents.[1,2] A number of groups have examined the thermal decomposition of DMMP on metal oxides and oxide-supported catalysts.[3−7] Klabunde and co-workers have extensively examined the application of nanoparticulate metal oxide materials for these applications.[8−11] Most of these studies have been concerned with decomposition reactions at temperatures in excess of 100−150 °C that are appropriate for decomposition or detoxification applications that allow for high temperatures. These applications include demilitarization of chemical warfare agent (CWA) stockpiles, incinerator emission cleanup, or fixed installation air filtration/decontamination systems. Low-temperature studies of the adsorption and thermal decomposition reactions of DMMP on solid oxides or supported catalysts have also been carried out.[12−17] The development of materials that are reactive for the decomposition of CWAs at low temperatures is important because of the need for the protection of personnel in the field, where access to power supplies or water may be limited. Applications include personal protection devices such as gas masks, additives to fabrics to provide active protection against toxic compounds, as well as materials that can be used to decontaminate surfaces and equipment that have been exposed to CWAs. Materials that are developed for these applications have the potential for dual use, providing technology that may be effective for the protection of personnel involved in hazardous materials cleanup and disposal. However, finding solid materials that exhibit decomposition capacities at low temperatures that are higher than that of pure alumina has proven difficult.

In this paper, we report results obtained from a new supported, coimpregnated cerium and iron oxide adsorbent that shows significantly enhanced decomposition activity at ambient temperatures compared to materials examined earlier, including pure alumina, and discuss possible reasons for this increased activity based on characterization of the adsorbents.

DMMP decomposition reactions that occur on solid surfaces at room temperature are stoichiometric as opposed to catalytic,[18] even when the process is a photoactivated one,[19] as in the case of titania surfaces,[20,21] with the nonvolatile, phosphorus-containing fragments left at the active decomposition sites effectively poisoning the sites for further decomposition. In a previous study of the DMMP decomposition reaction at room temperature,[13] it was found that materials such as a commercial γ-Al_2O_3 (150 m^2/g) and a supported iron oxide on alumina (FeO_x/Al_2O_3) decomposed approximately 100 μmol of DMMP per gram of solid. A sol−gel Al_2O_3 formulation (250 m^2/g) was about twice as effective, decomposing 200 μmol of DMMP per gram, presumably due to its higher surface area and the presence of more reactive transitional alumina phases. The extent of decomposition was measured by the evolution of gas-phase products, primarily methanol along with minor amounts of dimethyl ether, assuming that each molecule of methanol produced corresponded to one DMMP molecule decomposed and each dimethyl ether corresponded to two molecules decomposed. The decomposition is thought to proceed via

* Corresponding author. E-mail: mmitchel@cau.edu.

10.1021/jp021836m CCC: $25.00
Published on Web 12/17/2002

cleavage of one of the phosphorus−methoxy bonds, followed by the evolution of the methoxy group as methanol.[22] Dimethyl ether is thought to be formed as a secondary product, from the acid-catalyzed dehydration of methanol.[13]

In situ infrared spectroscopy shows that alumina-supported iron oxide is more reactive for DMMP decomposition than alumina alone, at least with regard to the initial adsorption sites.[23] However, the overall capacity of alumina-supported iron oxide to decompose DMMP appears to be somewhat less than that of pure alumina, as measured by the formation of volatile products.[13] It was thought that perhaps the inability of the iron oxide to convert surface-bound methyl or methoxy fragments to volatile products might be responsible for these apparent differences, and that an appropriate cocatalyst could convert the adsorbed fragments to volatile products.

In the current study, the activities of cerium- and iron-coimpregnated oxides for room-temperature DMMP decomposition are examined. It was decided to add cerium to the alumina-supported iron oxide material to determine if the ability of cerium to act as an oxygen storage material could increase the decomposition capacity of the solid. The total DMMP decomposition, as measured by volatile product formation, is determined for several different $FeO_x/CeO_y/Al_2O_3$ formulations, including different loadings of iron and cerium oxides by themselves on alumina, and in different relative amounts, and formed into combined supported oxide adsorbents by impregnating the iron and cerium in separate steps, and simultaneously. It is shown that the coimpregnated oxides show significantly increased capacity for the conversion of adsorbed DMMP to volatile products.

Experimental Section

The helium used for the study was a 99.9995% ultrahigh purity grade from Holox. DMMP was purchased from Aldrich and distilled under vacuum before use. The adsorbents are prepared using incipient wetness, with iron and cerium nitrates as the precursors and deionized water as the solvent. The alumina used was a γ-Al_2O_3 provided by UOP with a surface area of approximately 253 m^2/g. The metals content of each sample was determined using ICP-MS (Perkin-Elmer Elan 5000).

Microreactor Studies. The microreactor system has been described in detail previously.[13] Briefly, the microreactor consists of a 1/4" o.d. stainless steel U-tube in a controlled-temperature furnace, which is connected to a gas inlet system that carries the DMMP/He mixture to the reactor, and an exit system that carries the products to a 2.4 m long-path infrared gas cell for analysis. The inlet helium gas flow is controlled by a Teledyne-Hastings mass flow controller. The helium gas bubbles through liquid DMMP at a flow rate of 30 mL/min. The DMMP concentration in the He stream has been determined to be 30.25 μmol/L. At a flow rate of 30.0 mL/min, the flow rate of DMMP was determined to be 0.908 μmol/min.

For reaction studies, the adsorbent (~60 mg) was placed near the bottom of the "U" but on the entrance side. Unlike our earlier studies, the adsorbent bed is composed of relatively larger particles (90−250 μm diameter, classified using standard testing sieves), and sits on a porous stainless steel disk with 2 μm diameter pores. A type-K thermocouple in the adsorbent bed provided the temperature feedback to the Omega process control unit. After the adsorbent bed, the gas mixture flowed to a long-path gas cell (Ultra-Mini Long Path Cell from Infrared Analysis, Inc.) with an effective path length of 2.4 m and an internal volume of 100 mL. Infrared spectra, at 2 cm^{-1} resolution, were collected approximately every two minutes. The data analysis was carried out as in the earlier study.

All solids for the reaction studies were pretreated by heating in flowing O_2 (20% O_2 in Helium) for 1 h at 400 °C followed by heating in flowing He at 400 °C for 1 h. The sample was then cooled to the reaction temperature in flowing He.

X-ray Diffraction Measurements. Powder X-ray diffraction measurements were performed on a Philips PW 1800 X-ray Diffractometer with a Cu Kα source at 1.54 Å, operated at 40 kV and 30 mA, using a step size of 0.04 (2θ).

FT-Raman Measurements. FT-Raman spectra were obtained using a Nicolet Raman 950 FT-Raman spectrometer. The instrument uses a Nd−VO_4 laser, and was operated at a power of approximately 250 mW. Raman scattered radiation was collected using a 180° backscattering collection geometry and detected using a room-temperature InGaAs detector. The neat powder samples were placed in capillary tubes for data collection.

Infrared Diffuse Reflectance Studies. Before study, the alumina and the alumina-supported metal oxides were calcined at 500 °C in air in a muffle furnace for 24 h, and were stored in sealed containers in a desiccator prior to use. The pure solid being examined was sieved and placed in a Harrick Scientific HVC-DR infrared diffuse reflectance-controlled environment cell, and the spectra were collected using a Harrick Scientific DRA-2 optical accessory. The cell was closed and evacuated using an Alcatel diffusion pump and heated to 50 °C under vacuum to remove adsorbed water. After cooling to room temperature under vacuum, a dilute mixture of DMMP in helium (1:1000) was allowed to flow through the cell. The pressure in the cell during this time was approximately 500 mTorr. Spectra were measured during the adsorption process to monitor for DMMP adsorption using a Nicolet Magna 750 FT-IR and a liquid nitrogen cooled mercury-cadmium-telluride (MCT) detector. During adsorption, 250 scans at 8 cm^{-1} resolution (to minimize collection time) were co-added to form the spectra.

Results and Discussion

The measured reaction products from the study of the alumina substrate are shown in Figure 1. The accumulated flow of DMMP through the adsorbent bed, in μmoles, is the horizontal axis in the plots. This has been corrected for the volume of the reactor and tubing as discussed previously.[13] The vertical axis corresponds to the flow rate of the products observed (μmol/min), Figure 1A, or to the total accumulated flow of volatile carbon species produced by the reaction (μmoles), Figure 1B. ("All" represents the total number of μmoles of carbon produced by the reaction that appeared as volatile products, equal to two times the flow of dimethyl ether plus the flow of methanol at this temperature). As can be seen in Figure 1A, dimethyl ether was the first product at the infrared cell. Figure 1B shows the accumulated product formation as a function of DMMP flow, and represents the integration of Figure 1A.

The curves shown in Figure 1 are typical of the product flows observed for these materials. They are characterized by an induction period, a rapid rise in product flow up to a maximum, followed by a slower decrease in flow rate. Product formation continues for a relatively long period at a low rate until it is no longer possible to determine the product concentration above the noise. This alumina shows an induction period that is about twice that observed in our earlier studies of DMMP decomposition on similar solids.[13] The induction period is due, at least in part, to adsorption of methanol and dimethyl ether onto the surface of the adsorbent, and the longer induction period is a

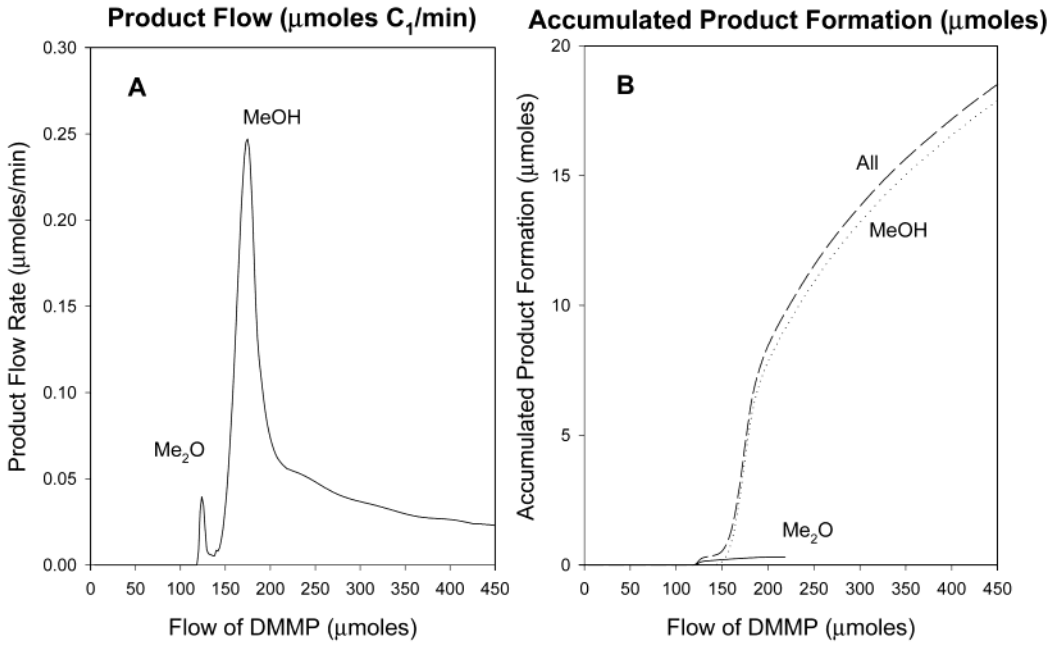

Figure 1. Results from the decomposition of DMMP on γ-alumina at 25 °C. Figure 1A shows the flow rate of products as μmol C_1/min. "μmoles of C1" means the equivalent number of one-carbon products, that is two times the number of μmol/min (or μmoles) of dimethyl ether plus the number of μmol/min (or μmoles) of methanol. Figure 1B shows the accumulated reaction products that have been measured in the gas phase. "All" represents the μmoles of C_1 products observed.

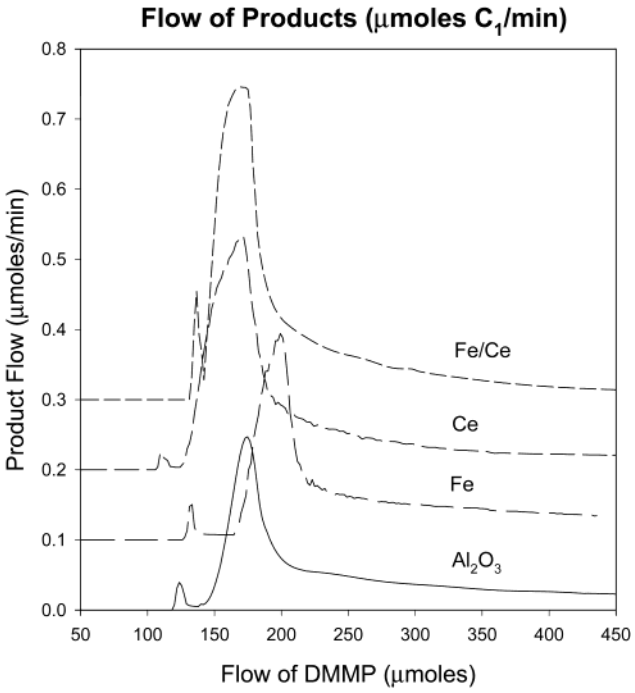

Figure 2. Product flow curves from the decomposition of DMMP at 25 °C on Al_2O_3, 5 wt % Fe on Al_2O_3, 7.5 wt % Ce on Al_2O_3, and 5 wt % Fe/7.5 wt % Ce on Al_2O_3. The curves are referenced to the same vertical scale, except that they have been offset to aid viewing. The initial baseline of each curve corresponds to its zero on the vertical scale.

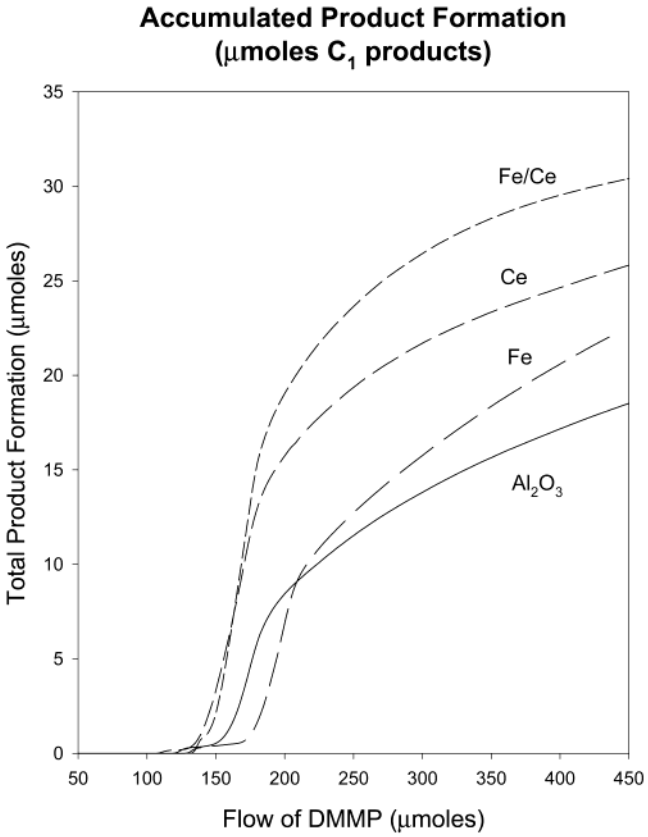

Figure 3. Accumulated product formation curves from the adsorption of DMMP at 25 °C on Al_2O_3, 5 wt % Fe on Al_2O_3, 7.5 wt % Ce on Al_2O_3, and 5 wt % Fe/7.5 wt % Ce on Al_2O_3.

consequence of the higher surface areas of the solids examined in the current work. The DMMP breakthrough point is also determined for the solids, and this is also predominantly a function of the surface area of the solids.

Figures 2 and 3 show the rate of product formation (product flow rate vs total DMMP flow) and the accumulated products formed, respectively, for alumina itself and for three impregnated alumina formulations, one containing 5 wt % iron, one containing 7.5 wt % cerium, and one containing 5 wt % Fe and 7.5 wt % Ce prepared using simultaneous impregnation. Because of the difference in atomic weights, the 7.5 wt % Ce sample has an atom coverage (atoms/nm^2) that is about 60% that of the 5

TABLE 1: Summary of the Screening Results

wt % Fe	wt % Ce	surface area (m^2/g)	DMMP breakthrough point (μmol DMMP)	maximum product formation rate (μmol/min)	total products formed (μmol)[a]
0	0	253	119	0.37	15
5	0	211	178	0.34	16+
5.5	2.52	229	168	0.41	17.5+
13.12	2.67	204	103	0.44	19
4.3	6.74	204	101	0.40	24
4.65	7.34	211	148	0.47	25
9.34	13.53	175	98	0.54	18
4.73	14.68	193	104	0.55	21

[a] After a flow of 240 μmoles of DMMP.

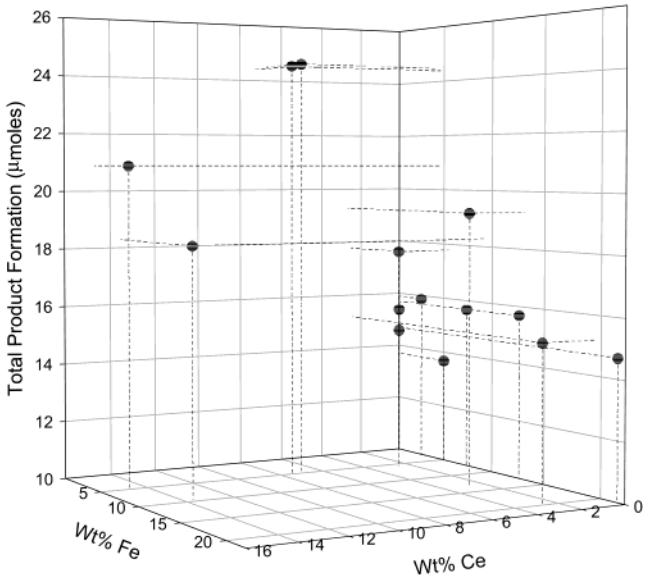

Figure 4. Results from the screening experiments using different compositions of iron and cerium oxide supported on aluminum oxide.

wt % Fe sample. The mole ratio, Fe:Ce, for the 5 wt % Fe/7.5 wt % Ce sample is 1.67:1. All three impregnated materials show increased product flow and total product yield compared to the unimpregnated alumina, but the performances differ. Since the product flow tends to be more variable than the total product yield for the different adsorbents, probably due to differences in flow through the adsorbent bed, the total product yield was chosen to be the metric by which the different adsorbents are judged.

A range of adsorbents prepared using simultaneous impregnation with different iron and cerium contents were examined for their ability to decompose DMMP. The total weight loading in the materials examined was kept below about 20 wt % for the total loading of iron plus cerium, although one sample examined turned out to have a total weight loading of slightly less than 23 wt %. To be able to conduct the experiments in a reasonable period of time, a screening protocol was established that used the amount of products formed after exposure to 240 μmol of DMMP as the performance measure. The characteristics of the different adsorbents examined and their product yields are given in Table 1. The total decomposition yield results were then plotted as a function of Fe and Ce content, and the resulting graph is shown in Figure 4.

The 1.67:1 mole ratio of Fe/Ce (5 wt % Fe/7.5 wt % Ce) gave the best results of the materials examined. This result has been consistently observed for several different batches of adsorbents that have been synthesized and their activities compared.

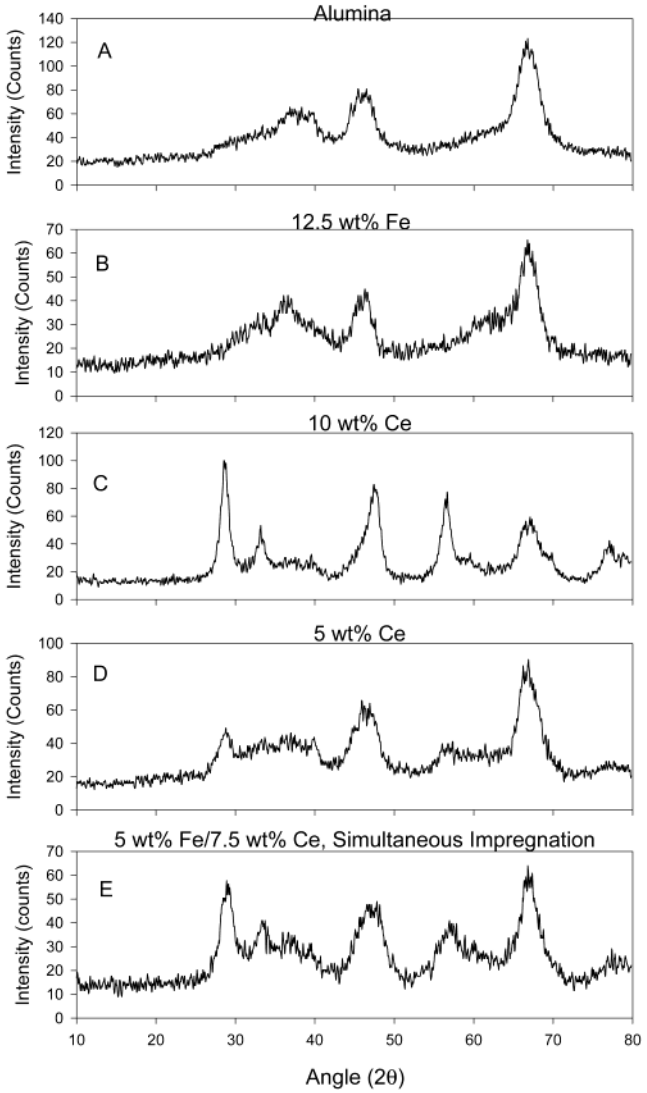

Figure 5. Powder X-ray diffraction patterns for alumina and alumina impregnated with iron and cerium. Figure A is the X-ray diffraction pattern for pure alumina, B is that for alumina impregnated with 12.5 wt % Fe, C is that for alumina impregnated with 10 wt % Ce, D is that for alumina impregnated with 5 wt % Ce, and E is that for 5 wt % Fe and 7.5 wt % Ce impregnated onto the alumina simultaneously.

Experiments were carried out to determine if the order of impregnation had an effect on the observed product yield. These experiments used adsorbents with the same gross composition, 5 wt % Fe/7.5 wt % Ce, but for one adsorbent the support was first impregnated with iron followed by calcining, then impregnated with cerium followed by calcining, while for another adsorbent, the impregnation order was reversed. The results indicated that impregnation with the cerium first and iron second yielded an adsorbent that showed a product yield slightly improved compared to an adsorbent containing iron alone, while one formed by impregnating with iron first and cerium second yielded an adsorbent that showed a product yield only slightly reduced compared to the adsorbent prepared by impregnating simultaneously. These results seem to indicate that cerium is the most important component of the mixed oxide.

Powder X-ray diffraction patterns for a series of alumina-supported materials are shown in Figure 5. As can be seen, the alumina by itself gives a pattern consistent with γ-Al_2O_3, and the addition of as much as 12.5 wt % iron adds nothing in the way of diffraction peaks to the pattern, suggesting that the

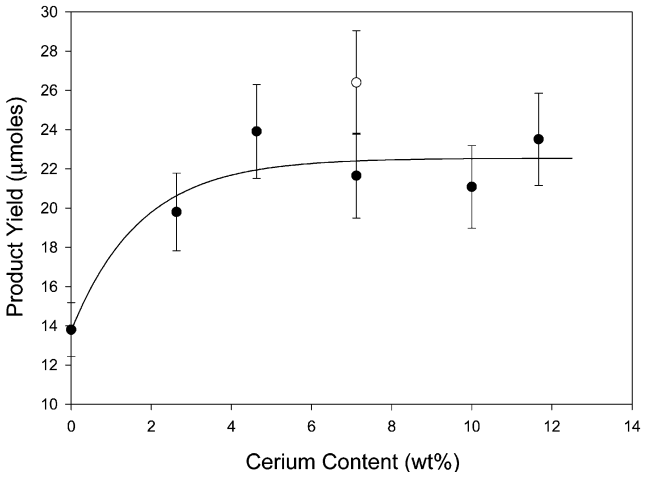

Figure 6. The product yield at 300 μmoles of DMMP exposure is shown as a function of cerium content for the cerium-only adsorbents. The hollow circle shows the product yield for the 5 wt % Fe/7.5 wt % Ce adsorbent (simultaneous impregnation) after exposure to the same amount of DMMP. The error bars represent estimates of the uncertainty in the yield determination. The line is a nonlinear regression fit of the cerium-only data to an exponential rise to a maximum.

alumina substrate acts as a template for the iron deposition. The addition of cerium, however, clearly results in the formation of additional peaks in the diffraction pattern, and these peaks are consistent with the formation of a CeO_2 phase.[24] The significant drop in intensity (more than a factor of 2) on going from 10 wt % Ce to 5 wt % Ce, suggests that the ceria is present on alumina as a crystalline phase and as an amorphous phase, and this will be further discussed later. The diffraction patterns for the adsorbents prepared by sequential impregnation (not shown) are virtually indistinguishable, whether cerium is impregnated first or second, and both show prominent features due to the CeO_2 phase. The features indicative of CeO_2 are relatively less intense and broader for the sample prepared using simultaneous impregnation, indicating less formation of the CeO_2 phase and/or smaller particle sizes for this phase.

Cerium-only Adsorbents. A series of experiments were carried out that examined the yield of decomposition products for a series of adsorbents containing cerium only. The results are shown in Figure 6. After the addition of as little as 2.5 wt % cerium, a significant increase in product yield is observed, which appears to plateau after the addition of a total of 5 wt % cerium. Included in Figure 6 is the data point that corresponds to the 5 wt % Fe/7.5 wt % Ce adsorbent prepared using simultaneous impregnation, showing a significantly higher decomposition yield than what is expected for an adsorbent with the same amount of cerium in a cerium-only adsorbent.

FT-Raman Studies. A band at 462 cm^{-1} that is observed in the FT-Raman spectra of the adsorbents is indicative of the presence of a CeO_2 phase for alumina-supported cerium oxide (see Figure 7).[24−26] This band has been assigned to the F_{2g} Raman active mode of CeO_2. Other features are present in the spectra of the supported cerium, but these peaks are only observed clearly at higher weight loadings. The only other notable feature in the FT-Raman spectrum is a very broad fluorescence background. The alumina support alone also shows a fluorescence background with no peaks, but the fluorescence background has a different wavelength dependence than that of the cerium-only samples. No peak at 462 cm^{-1} is observed for the 2.5 wt % Ce sample, and this spectrum is used to correct the other spectra for the fluorescence background, and the corrected spectra are shown in Figure 7. A plot of the intensity of the 462 cm^{-1} band as a function of cerium content is shown in Figure 8.

Wachs has suggested using Raman spectroscopy to determine the surface metal concentration that yields monolayer coverage for a supported metal oxide species.[27] Microcrystalline metal oxide species on supports and their monolayer counterparts often have distinct Raman bands, and typically the surface-bound species is formed first, through interaction with surface hydroxyls on the support. Once the more reactive surface hydroxyl groups have reacted, subsequent metal oxide species form on top of the surface species, yielding the microcrystals. Typical monolayer coverages for metal oxides on Al_2O_3 determined in this fashion vary from 2.3 atoms/nm^2 for rhenium to 7.3 atoms/nm^2 for vanadium, with Cr, Mo, W, and Nb all between 4.0 and 5.0 atoms/nm^2. From Figure 8 it is possible to estimate that the monolayer surface coverage of ceria on the alumina substrate occurs at a loading between 2.5 and 3 wt % Ce, approximately 0.4−0.5 atoms/nm^2.

Shyu et al. suggested that a breakpoint in their XPS results from a ceria/alumina material that occurred at a ceria loading of 2.6 μmol/m^2 (1.6 Ce atoms/nm^2) corresponded to the loading below which most of the ceria was present on the alumina surface as a "$CeAlO_3$ precursor".[25] They observed a Raman band for the CeO_2 phase at a surface concentration as low as 0.58 μmol/m^2, which corresponds to 0.35 Ce atoms/nm^2, similar to the limit that was observed above. This ceria found at low ceria loadings was observed to give XPS results similar to Ce^{3+}, and did not show a CeO_2 Raman spectrum, but was reducible in TPR experiments, so it could not correspond to a true $CeAlO_3$ phase. Martínez-Arias et al. determined, on the basis of XANES data, that the cerium species present at low alumina coverages must be due to a Ce^{4+} species.[24] These authors concluded that the most common form for the dispersed ceria phase is as two-dimensional patches or networks of ceria. Their UV−vis diffuse reflectance spectra were not consistent with the formation of large numbers of isolated cerium ions on the alumina surface. Their EPR results also supported this interpretation. They suggested that the interatomic distances in the 2-dimensional ceria patches are expanded in relation to distances found in 3-dimensional crystals.

From the current FT-Raman results, it appears that the monolayer phase is complete after the addition of slightly more than 2.5 wt % Ce, and that additional cerium produces CeO_2. The cerium-only decomposition results show that most of the increase in decomposition capacity for these adsorbents occurs for weight loadings less than 5 wt %, before a significant amount of the CeO_2 phase has been formed. Also, a plateau in the decomposition yield is observed for cerium loadings that simultaneously show an increasing contribution from the CeO_2 phase. These results clearly indicate that the CeO_2 phase is not the active phase on the support, but that a dispersed cerium oxide phase present on the support prior to the formation of the distinct CeO_2 phase is the component important for decomposition of DMMP. This phase is probably in the form of two-dimensional patches or networks as suggested by Martínez-Arias et al.[24]

Effect of Iron. The concentration of cerium on the surface that apparently represents the maximum concentration for monolayer formation, approximately 0.4 atoms/nm^2, is relatively low to lead to the formation of a three-dimensional phase, given the typical site densities (OH's, anion vacancies, or oxygen atoms), in the neighborhood of 5 sites/nm^2, on alumina surfaces,[28] and as compared to the typical monolayer metal

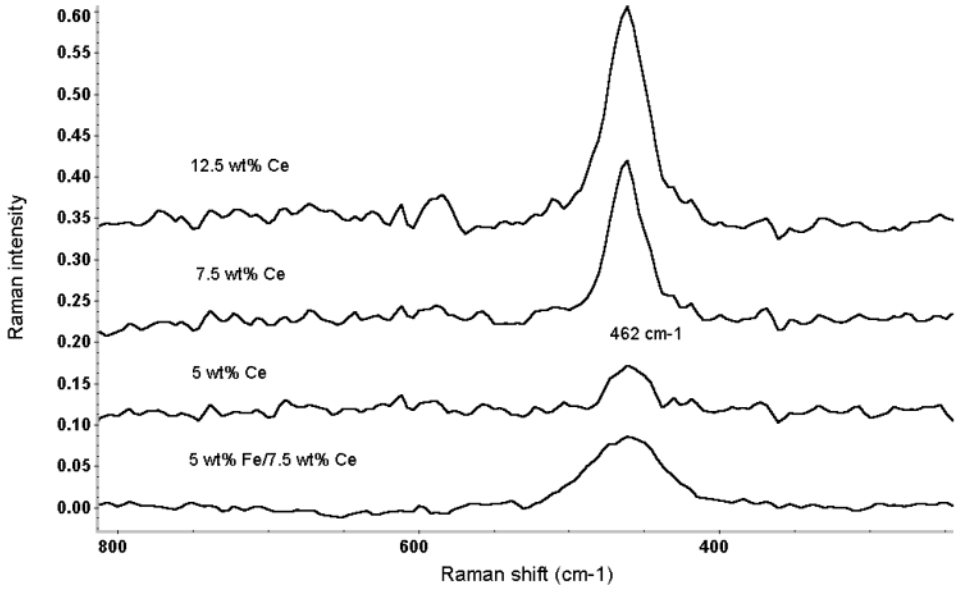

Figure 7. FT-Raman spectra of cerium-only adsorbents as a function of cerium content. The spectra are shown with a common vertical scale, except for the baseline offset to aid viewing. The baseline in each spectrum corresponds to its zero on the vertical scale.

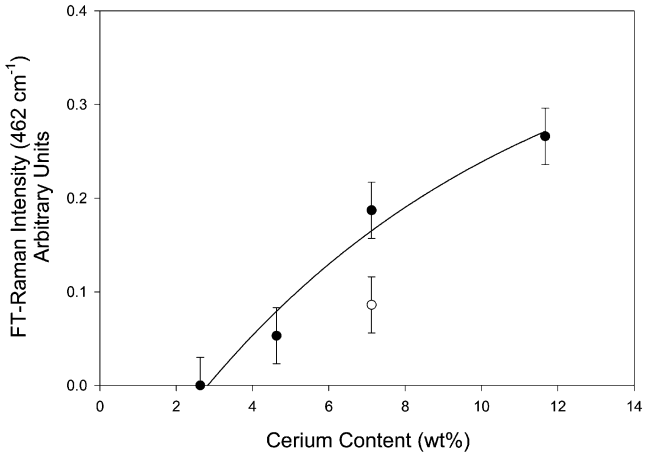

Figure 8. Plot of the FT-Raman intensity of the CeO_2 band at 462 cm^{-1} vs cerium content. The filled circles represent the data from the cerium-only adsorbents and the hollow circle is the data point from the 5 wt % Fe/7.5 wt % Ce adsorbent (simultaneous impregnation). The curve shown on the plot is included as a guide to the approximate behavior of the intensity as a function of Ce loading on the samples, and is not based on any model of Raman intensity as a function of CeO_2 concentration for powder samples.

coverages referred to above for other oxides on alumina. This suggests that the active (dispersed) cerium oxide phase is unstable on the alumina surface, and suggests one possible mode for the enhancement effect of iron.

FT-Raman spectroscopy also provides important information with regard to the Fe/Ce mixed oxide material. Included in Figure 8 is the data point that corresponds to the intensity of the CeO_2 band for the 5.0 wt % Fe/7.5 wt % Ce material prepared using simultaneous impregnation. The intensity of the band for this material is approximately a factor of 2 less than that for the 7.5 wt % Ce-only adsorbent. This could lead to the conclusion that the iron caused a greater dispersion of the cerium oxide on the surface of the support, a larger fraction of the cerium oxide in the form of two-dimensional patches, which could account for the greater decomposition capacity.

However, a closer inspection of the spectra alters that conclusion somewhat. Included in the series of FT-Raman spectra in Figure 7 is the Raman spectrum of the 5.0 wt % Fe/7.5 wt % Ce-supported mixed oxide material. It is apparent in these spectra that the width of the CeO_2 band for the mixed oxide material is significantly larger than that of the cerium-only adsorbents. In fact, the full width at half-maximum (fwhm) for the CeO_2 band is 29 ± 3 cm^{-1} for the cerium-only adsorbents and nearly twice that value, 55 cm^{-1}, for the coimpregnated iron and cerium oxide material. Thus, the integrated area of the 462 cm^{-1} band is approximately equal for the two materials, the band for the cerium-only material has an integrated area about 10% greater than that of the coimpregnated oxide, but the peak intensity is lower for the coimpregnated oxide and the band is significantly wider. This is consistent with the interpretation that although there appears to be about as much of a contribution from the CeO_2 phase on the coimpregnated oxide adsorbent as on the cerium-only material, either the CeO_2 phase on the coimpregnated oxide is much less well-ordered, and probably contains many more defect sites than the cerium-only material, or the CeO_2 particles are much smaller, which also would yield a higher defect site density.[29,30] Although the cerium content is almost identical for these two materials, the amount of cerium present in a well-ordered CeO_2 phase has decreased due to the presence of iron.

This picture is also consistent with the results found for separate iron and cerium impregnation. If the cerium is deposited first, the active Ce oxide phase is partially obscured by the iron oxide phase deposited on top, yielding an adsorbent that is slightly more active than the alumina impregnated with iron oxide alone. If the iron oxide is deposited first, the iron oxide forms a surface on the alumina that is very similar to the alumina surface, as far as the cerium is concerned, and the resulting adsorbent yields results similar to those found for the cerium-only adsorbent.

Some speculation is possible on the nature of the increased decomposition capacity observed for the cerium-containing materials. As has been clearly described in a recent review by Trovarelli, cerium is a very effective oxidation catalyst.[31] Badri et al.[32] found that methanol dissociates at room temperature on high surface area ceria samples calcined in O_2 at 400 °C. The methoxy surface coverage observed was 4.2 methoxy groups per nm^2, close to monolayer coverage. Its ability to oxidize CO has been linked to its ability to activate adsorbed O_2 as the superoxide O_2^-. Its ability to activate CH_4 is thought to involve

labile lattice oxygen atoms, involving the cerium Ce^{4+}/Ce^{3+} redox cycle, eq 1:[31,33]

$$CeO_2 \leftrightarrow CeO_{2-x} + xO \quad (1)$$

Given the experimental protocol used in the experiments reported here, it is very unlikely that O_2^- participates in the decomposition reaction of DMMP. Both Soria et al.[34] and Martínez-Arias et al.[24] have shown that O_2^- species bound to dispersed ceria are much more weakly bound than similar species bound to three-dimensional CeO_2, and are eliminated by outgassing at room temperature. This virtually eliminates this type of oxygen from being an important contributor in our experiments since they all involve outgassing at room temperature before DMMP exposure. Thus, the mode of action of the ceria in these experiments probably involves participation of lattice oxygen as in the Mars and van Krevelen mechanism.[35] This is consistent with the work of Soria et al. who found that surface anion vacancies are more easily formed on dispersed ceria than on CeO_2 crystallites.[34] The Mars and van Krevelen mechanism was suggested as a possible DMMP decomposition mode in our earlier work,[12] but seems even more likely in these experiments.

Infrared diffuse reflectance measurements of the powdered adsorbent were obtained to examine the nature of the adsorbed species during reaction. The spectra were obtained in much the same way as described in an earlier publication.[12] A band at 2814 cm^{-1}, not due to adsorbed molecular DMMP,[3,12] was clearly observed, and was found to coincide with a band observed when methanol was allowed to contact alumina-supported cerium oxide, and was assigned to a methoxy group adsorbed on the surface. A similar band has been observed by Rusu and Yates in their work on titania surfaces.[14,21] The methoxy band appears simultaneously with the first DMMP bands, and increases in intensity with increasing DMMP exposure. However, the intensities of the DMMP bands increase faster than that of the methoxy band, so that the relative intensity of the methoxy band slowly decreases with DMMP exposure. A similar band is not observed upon DMMP adsorption on alumina,[3,23] an indication that the methoxy group that is formed during the decomposition is not stable on the alumina surface. The adsorbed methoxy group may, in fact, be the source of the increased ceria activity. The methoxy group formed from an initial DMMP adsorption/decomposition step may, instead of evolving from the surface as methanol, react with a second DMMP molecule initiating its decomposition. A future manuscript will address these questions.

Conclusion

We have examined the decomposition reaction of DMMP on a series of alumina-supported iron and cerium oxides at room temperature. These new materials decompose more than twice as much DMMP per gram as had been achieved using the most active alumina studied previously, a sol−gel alumina. A screening protocol demonstrated that the composition that yielded the greatest product formation, and the greatest degree of decomposition, contained 5.0 wt % iron and 7.5 wt % cerium, prepared by impregnating the alumina simultaneously with iron and cerium precursors. Correlating the FT-Raman results with the product formation yields for cerium-only adsorbents suggests that the active component for DMMP decomposition is a two-dimensional ceria network on the alumina support. Previous work by others has suggested that two-dimensional ceria networks are better able to make lattice oxygen available than the three-dimensional networks, and it is proposed here that it is the lattice oxygen which then reacts with DMMP, ultimately resulting in the formation of methanol and/or dimethyl ether that evolve as gas-phase products. The FT-Raman results suggest that the effect of iron is to increase the number of ceria defect sites in the crystallites that do form by disrupting the crystal structure and/or facilitating the formation of smaller particles.

Acknowledgment. The authors gratefully acknowledge Dr. Alexei Iretski of the Georgia Institute of Technology for acquiring the X-ray diffractograms. The authors thank the U. S. Army, Edgewood Chemical Biological Center, for support of this research through contract number DAAD13-99-C-0010. Also, the authors acknowledge the support of NASA through grant number NCC3-552.

References and Notes

(1) Ekerdt, J. G.; Klabunde, K. J.; Shapley, J. R.; White, J. M.; Yates, J. T., Jr. *J. Phys. Chem.* **1988** *92*, 6182.
(2) Bowen, J. M.; Powers, C. R.; Ratcliffe, A. E.; Rockley, M. G.; Hounslow, A. W. *Environ. Sci. Technol.* **1988**, *22*, 1178.
(3) Mitchell, M. B.; Sheinker, V. N.; Mintz, E. A. *J. Phys. Chem. B* **1997**, *101*, 11192.
(4) Graven, W. M.; Weller, S. W.; Peters, D. L. *Ind. Eng. Chem Process Des. Dev.* **1966**, *5*, 183.
(5) Tzou, T. Z.; Weller, S. W. *J. Catal.* **1993**, *146*, 370.
(6) Lee, K. Y.; Houalla; M. Hercules, D. M.; Hall, W. K. *J. Catal.* **1994**, *145*, 223.
(7) Cao, L.; Segal, S. R.; Suib, S. L.; Tang, X.; Satyapal, S. *J. Catal.* **2000**, *194*, 61.
(8) Li, Y. X.; Schlup, J. R.; Klabunde, K. J. *Langmuir* **1991**, *7*, 1394.
(9) Li, Y. X.; Klabunde, K. J. *Langmuir* **1991**, *7*, 1388.
(10) Li, Y. X.; Koper, O.; Atteya, M.; Klabunde, K. J. *Chem. Mater.* **1992**, *4*, 323.
(11) Jiang, Y.; Decker, S.; Mohs, C.; Klabunde, K. J. *J. Catal.* **1998**, *180*, 24.
(12) Tesfai, T. M.; Sheinker, V. N.; Mitchell, M. B. *J. Phys. Chem. B* **1998**, *102*, 7299.
(13) Sheinker, V. N.; Mitchell, M. B. *Chem. Mater.* **2002**, *14*, 1257.
(14) Rusu, C. N.; Yates, J. T., Jr. *J. Phys. Chem. B* **2000**, *104*, 12292.
(15) Templeton, M. K.; Weinberg, W. H. *J. Am. Chem. Soc.* **1985**, *107*, 97.
(16) Templeton, M. K.; Weinberg, W. H. *J. Am. Chem. Soc.* **1985**, *107*, 774.
(17) Aurian-Blajeni, B.; Boucher, M. M. *Langmuir* **1989**, *5*, 170.
(18) Li, Y. X.; Klabunde, K. J. *Langmuir* **1991**, *7*, 1388.
(19) Segal, S. R.; Suib, S. L.; Tang, X.; Satyapal, S. *Chem. Mater.* **1999**, *11*, 1687.
(20) Obee, T. N.; Satyapal, S. *J. Photochem. Photobiol. A: Chem.* **1998**, *118*, 45.
(21) Rusu, C. N.; Yates, J. T., Jr. *J. Phys. Chem. B* **2000**, *104*, 12299.
(22) Templeton, M. K.; Weinberg, W. H. *J. Am. Chem. Soc.* **1985**, *107*, 97.
(23) Tesfai, T. M.; Sheinker, V. N.; Mitchell, M. B. *J. Phys. Chem. B* **1998**, *102*, 7299.
(24) Martínez-Arias, A.; Fernández-Garcia, M.; Salamanca, L. N.; Valenzuela, R. X.; Conesa, *J. Phys. Chem. B* **2000**, *104*, 4038.
(25) Shyu, J. Z.; Weber, W. H.; Gandhi, H. S. *J. Phys. Chem.* **1988**, *92*, 4964.
(26) Larrson, P.-O.; Andersson, A. *J. Catal.* **1998**, *179*, 72.
(27) Wachs, I. E. *Catal. Today* **1996**, *27*, 437.
(28) Knozinger, H.; Ratnasamy, P. *Catal. Rev.-Sci. Eng.* **1978**, *17*, 31.
(29) Graham, G. W.; Weber, W. H.; Peters, C. R.; Usmen, R. K. *J. Catal.* **1991**, *130*, 310.
(30) Vlaic, G.; Di Monte, R.; Fornasiero, P.; Fonda, E.; Kaspar, J.; Graziani, M. *J. Catal.* **1999**, *182*, 378.
(31) Trovarelli, A. *Catal. Rev.* **1996**, *38*, 439.
(32) Badri, A.; Binet, C.; Lavalley, J. C. *J. Chem. Soc., Faraday Trans.* **1997**, *93*, 1159.
(33) Kundakovic, Lj.; Flytzani-Stephanopoulos, M. *J. Catal.* **1998**, *179*, 203.
(34) Soria, J.; Coronado, J. M.; Conesa, J. C. *J. Chem. Soc., Faraday Trans.* **1996**, *92*, 1619.
(35) Mars, P.; Van Krevelen, D. W. *Chem. Eng. Sci. Suppl.* **1954**, *3*, 41.